Aerospace Science and Technology 58 (2016) 103–115

Contents lists available at ScienceDirect

Aerospace Science and Technology

www.elsevier.com/locate/aescte

Parameters effect of pulsed-blowing over control surface

Yankui Wang [a,b,1], Ping Zhou [a,b,*,2], Jiaji Yang [a,b,3]

[a] Ministry-of-Education Key Laboratory of Fluid Mechanic, Beihang University, Beijing 100191, China
[b] The School of Aeronautic and Engineering, Beihang University, Beijing 100191, China

ARTICLE INFO

Article history:
Received 23 March 2016
Received in revised form 9 August 2016
Accepted 11 August 2016
Available online 16 August 2016

ABSTRACT

Control surface, which is often located in the trailing edge of wings, is important in the attitude control of an aircraft. However, the efficiency of the control surface declines severely under the high deflect angle of the control surface because of the flow separation. To improve the efficiency of control surface, this study discusses a novel flow control technique aimed at suppressing the flow separation by pulsed blowing at the leading edge of the control surface. Results indicated that flow separation over the control surface can be suppressed by pulsed blowing, and the maximum average pitching moment coefficient of the control surface can be increased by nearly 90% when average blowing momentum coefficient is 0.03 relative to that of without blowing. Moreover, the lift coefficient of the control surface can be 95% times higher than that of without blowing, and the drag coefficient of the control surface can be reduced by 43% compared with that of without blowing. Finally, this study shows that the average blowing momentum coefficient and non-dimensional frequency of pulsed blowing are two of the key parameters of the pulsed blowing control technique. Both experimental and numerical simulations are used in this study. The experiment is completed in D-4 wind tunnel of Beihang University under conditions of Re 0.8×10^6.

1. Introduction

Control surface, which is often located in the trailing edge of wings, is important in the attitude control of an aircraft. However, the efficiency of the control surface declines severely under the high deflect angle of the control surface because of the flow separation (see Fig. 1). This condition leads to the penalty of attitude control and limited aerodynamic performance of an aircraft. Therefore, suppressing the flow separation is considered in this study.

Flow control [1] is the most available approach to achieve the goal of suppressing flow separation. In the past decades, scientists have exerted considerable effort to develop flow control techniques. Moreover, various flow control techniques have been used to suppress flow separation such as moving surface control technique [2–4], plasma flow control technique [5–8] and co-flow jet control technique [9–12]. Although flow separation on the control surface can be suppressed substantially by moving surface control technique or plasma flow control technique, the application of these techniques in engineering is limited because of complicated devices. For the co-flow jet control technique, a large amount of gas is necessary to suppress the flow separation. Thus, a powerful device is required to supply a high mass flow rate of jet. Recently, Wang et al. [13] developed a micro-blowing flow control technique to suppress the flow separation and improve the aerodynamic efficiency of the control surface.

Wang et al. set a blowing airfoil (see Fig. 2) based on NACA0025 to demonstrate the micro-blowing flow control technique. A blowing slot that is normal to the boundary of flap was set near the leading edge of the flap. A high energy jet parallel to the upper surface of flap is injected to the main flow. The study shows that the flow separation can be suppressed by blowing at the leading edge of the flap. Moreover, the study shows that the maximum increment of lift coefficient of the flap can be 150%, while AOA (angle of attack) of the main wing is 0°, the deflection angle of flap is 20° and the Reynolds number is 0.8×10^6. Wang et al. considered pulsed blowing to reduce the considerable gas requirement. Even though several researchers have also made improvements in development of the pulse jet technique to control the flow separation over the control surface [14,15], such technique is considerably more difficult to adopt in engineering because of lack of profound understanding of the fundamental mechanism and parameter similarity.

This study introduces an innovative flow control technique by pulsed blowing near the leading edge of the control surface to suppress the flow separation over the control surface that is located on the tailing edge of an airfoil. First, the effect of continuous

* Corresponding author.
E-mail addresses: wangyankui@buaa.edu.cn (Y. Wang), shakazp@163.com (P. Zhou), sanqiu66@126.com (J. Yang).
[1] Professor.
[2] PhD student.
[3] Master student.

http://dx.doi.org/10.1016/j.ast.2016.08.009
1270-9638/

Nomenclature

C_μ	average blowing momentum coefficient	C_{m-p}	average pitching moment coefficient of the flap generated by pressure
$C_{\mu t}$	instant blowing momentum coefficient	C_{D-p}	average drag coefficient of the flap generated by pressure
V_∞	velocity of the freestream ..... m/s	C_L	total average lift coefficient of the flap
Re	Reynolds number based on chord length of model	C_m	total average pitching moment coefficient of the flap
c_0	chord length of the model ..... m	C_D	total average drag coefficient of the flap
m_j	mass flow rate of blowing..... kg/s	C_{Lt}	instant lift coefficient of flap
V_j	jet velocity from the blowing slot..... m/s	c	chord length of flap ..... m
S_e	reference area of the control surface..... m^2	ρ_∞	density of free stream..... kg/m^3
S_j	area of the blowing slot..... m^2	α	attack angle of main wing..... °
f	frequency of pulsed blowing ..... Hz	δ_e	deflect angle of flap ..... °
Str	non-dimensional frequency of pulsed blowing	δ_j	angle between blowing jet and freestream..... rad
h_j	width of the blowing slot ..... mm	y'	the vertical distance from the surface of flap..... m
C_p	pressure coefficient		
C_{L-p}	average lift coefficient of the flap generated by pressure		

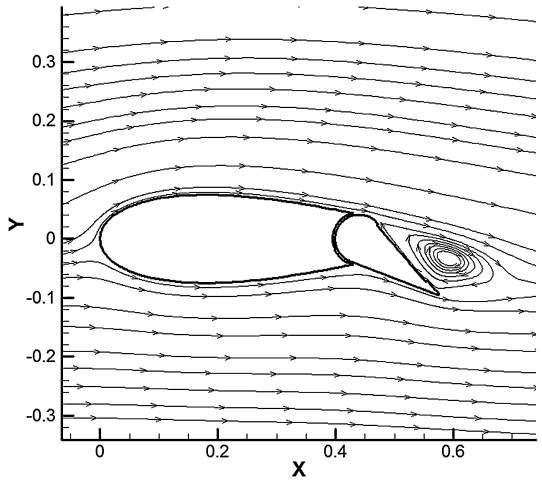

Fig. 1. Flow separation over the control surface ($\alpha = 0°$, $V_\infty = 20$ m/s, $\delta_e = 35°$).

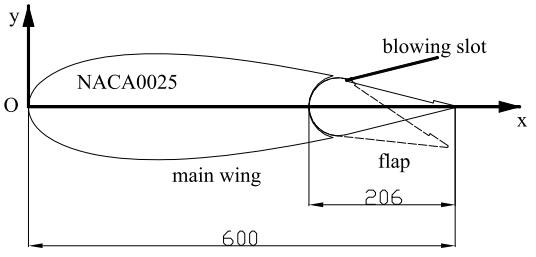

Fig. 2. Sketch of the blowing slot.

blowing on the suppression of the flow separation over the flap is mentioned briefly. Thereafter, the effect of pulsed blowing on the aerodynamic performance of the flap is investigated thoroughly. Furthermore, the mechanism of lift enhancement by pulsed blowing is discussed. All the results of this study are completed based on the following conditions: the AOA of the main wing is 0° and the deflect angle of the flap is 20°.

2. Experimental facilities and data processing

2.1. Wind tunnel and measurement device

The experiment is conducted in the D-4 low-speed wind tunnel of Beihang University (see Fig. 3), which has a 1.5 m × 1.5 m square test section and 2.5 m length. The velocity of the D-4 low-speed wind tunnel can be changed from 0 to 80 m/s with a turbulence level of 0.08%.

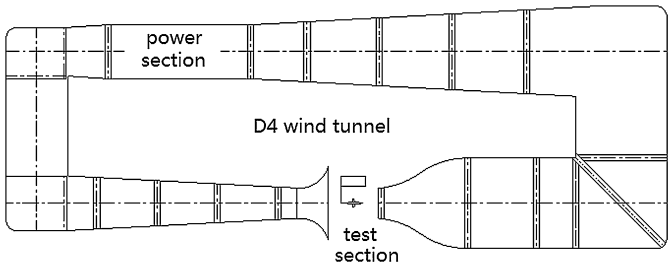

Fig. 3. Sketch of the D4 wind tunnel.

The DTC initium electronic scanner valve (see Fig. 4) is used to measure the pressure distribution of the model with an accuracy of 0.05% and the highest sampling frequency is 650 Hz.

A flow map DPIV system is used to acquire the velocity and vorticity fields over the flap. This system comprises four parts: a double-pulsed Nd:YAG laser, a four-megapixel CCD camera, a synchronization, and frame-grabber cards. The adaptive correlation, which uses iterations to offset the second window for cross-correlation analysis, is applied to calculate the velocity fields. The correlations are calculated using fast Fourier transform (FFT). The size of the interrogation windows is 32 × 32 pixels, and the overlapping interrogation windows in both directions are 25%. The corresponding spatial resolution is 3.1 mm. To reduce cyclic noise, the window function, which acts similar to an input filter to FFT, is selected as a Gaussian window. The filter used in the frequency domain prior to the inverse FFT is a low-pass Gaussian filter. The vorticity is solved using a normal second-order central difference, and the streamlines are parallel to the velocity vectors.

2.2. Model and blowing system

The airfoil model used in this study is based on NACA0025 (see Fig. 5). The model has 1 aspect ratio and 0.6 m the spanwise length. This model can be divided into two parts: the main wing and a control surface (flap) that is as long as 0.206 m. The flap can be deflected from −40° to 40° with a 5° interval. A spanwise blowing slot with a 0.5 mm height is located near the leading edge of the flap which is selected based on the flow separation point on the upper surface of the flap. Compressed air flows downstream along the tangential direction of the upper surface of the flap from the slot. The proposed model is equipped with 44 pressure taps at the longitudinal symmetric section along the upper and bottom

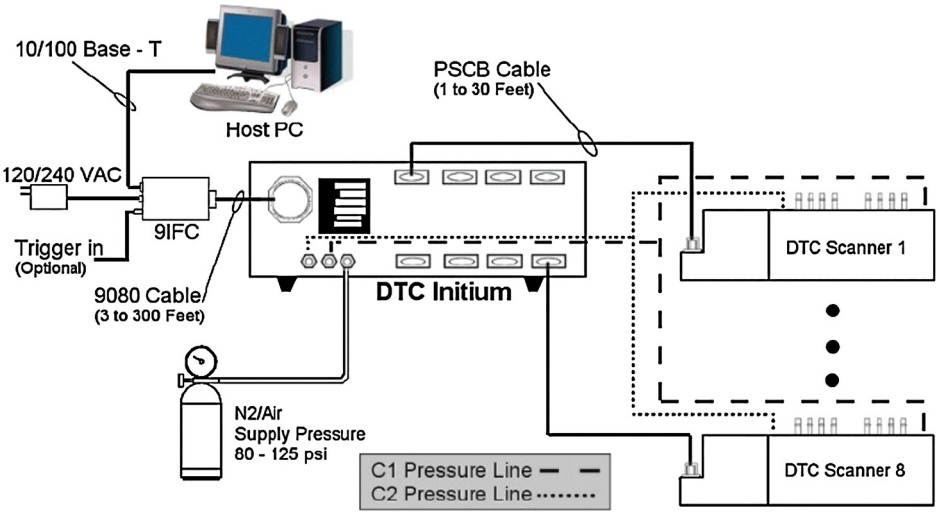

Fig. 4. Sketch of DTC pressure measurement system.

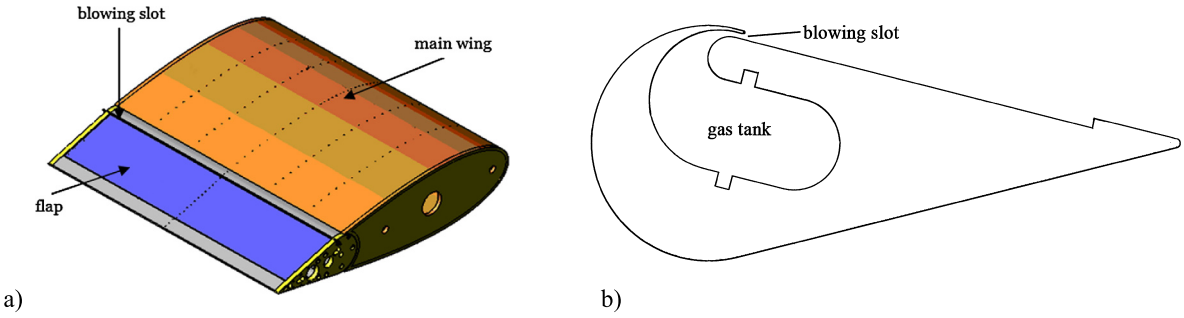

Fig. 5. Sketch of the experimental model for a) 3D model and b) flap section.

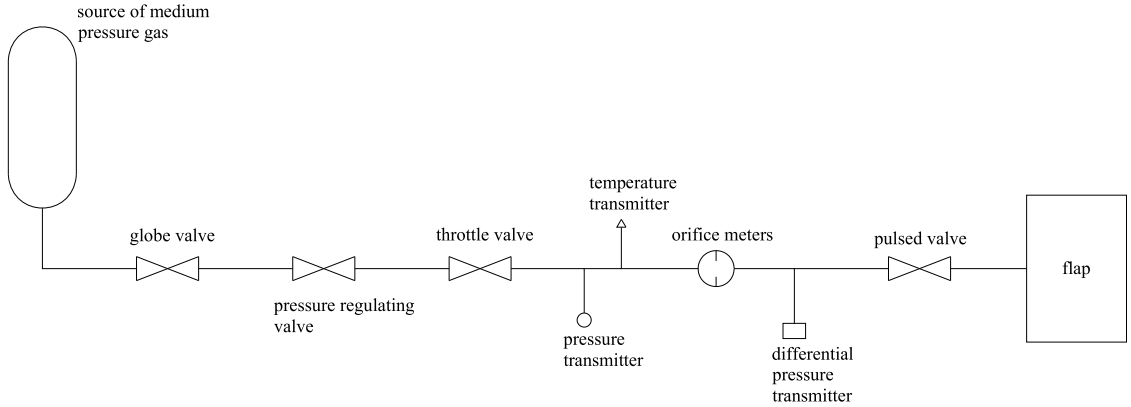

Fig. 6. Sketch of the blowing system.

flap. Two fiberglass plates are set on both sides of the model spanwise to simulate a two-dimensional flow in the test.

The blowing system is shown in Fig. 6. This system comprised three parts: the source of medium-pressure gas, measurement device of the mass flow rate, and pulse valve. The pulsed blowing equipment can theoretically provide sine-like wave with 72% duty cycle, and the frequency can be adjusted from 0 to 100 Hz. The typical wave of the pulsed blowing is illustrated in Fig. 7.

The 2D mesh of the model used in numerical simulation is as shown in Fig. 8. The minimum gap between the main wing and the flap is 0.5 mm, and the width of blowing slot is also 0.5 mm. An O-mesh with circle far-field, which is 20 chord length away from the model, is used in the simulation. In addition, the *k*-omega SST turbulence model is used. The boundary condition of the mass

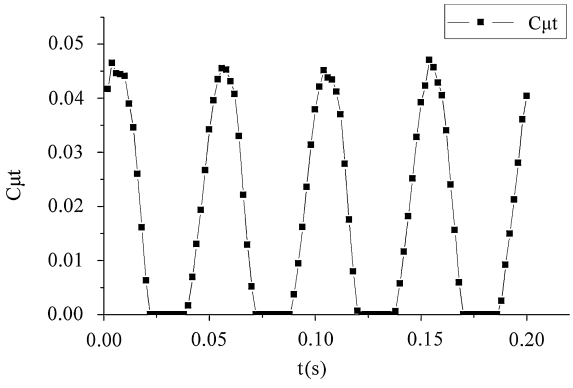

Fig. 7. Time history of pulsed blowing momentum coefficient in the experiment.

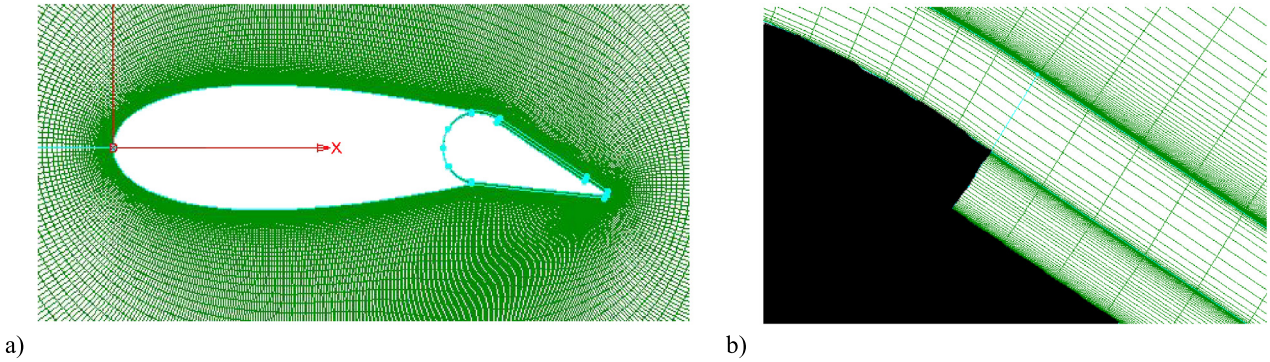

Fig. 8. Mesh of the numerical model for a) full model and b) blowing slot.

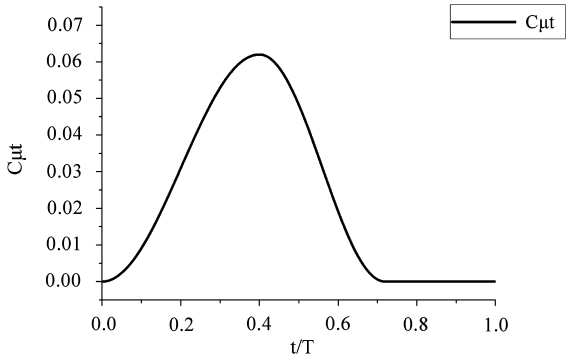

Fig. 9. Pulsed waveform used in the numerical simulation of the pulsed blowing.

flow rate is used on the blowing slot. The height of the first layer of the grid is 0.02 mm, and the number of cells is 79757.

The pulsed waveform used in the numerical simulation is similar to the waveform used in the experiment. This waveform is a sine-like wave with a 0.72 duty cycle but reaches its maximum at $t/T = 0.4$ (see Fig. 9).

2.3. Data processing

As the aerodynamic parameters are unsteady during a period of pulsed blowing, all of the aerodynamic parameters mentioned in this study are an average value of instantaneous value in one period. The reference center of the pitching moment coefficient is 0.15 m away from the leading edge of the main wing; this position can be approximately treated as the aerodynamic center of the model. Friction of the surface is not considered in this study because only pressure measurement test is used. The equations of the aerodynamic parameters in this study are as follows:

$$C_{m-p} = \frac{1}{T}\sum_{T}\left(\frac{\frac{1}{n}\sum_{1}^{n}(\oint_S \vec{r}_i \times \vec{p}_i d\boldsymbol{S})}{0.5\rho_\infty V_\infty^2 S_e c}\Delta t\right) \tag{1}$$

$$C_{L-p} = \frac{1}{T}\sum_{T}\left(\frac{\frac{1}{n}\sum_{1}^{n}(\oint_S -p_i \cos\theta_i d\boldsymbol{S})}{0.5\rho_\infty V_\infty^2 S_e}\Delta t\right) \tag{2}$$

$$C_{D-p} = \frac{1}{T}\sum_{T}\left(\frac{\frac{1}{n}\sum_{1}^{n}(\oint_S -p_i \sin\theta_i d\boldsymbol{S})}{0.5\rho_\infty V_\infty^2 S_e}\Delta t\right) \tag{3}$$

where c is the chord length of the flap. ρ_∞ is the density of freestream. S_e is the reference area of the flap. V_∞ is the velocity of freestream. $\vec{r}$ is the moment vector from the reference center to the pressure tap. $\vec{p}_i$ is the static pressure of the pressure tap. n is the number of taps. S is the surface of flap. $d\boldsymbol{S}$ is a vector normal to the interval between two adjacent taps. θ_i is the angle between the axis y and $d\boldsymbol{S}$. C_{m-p} is the pitching moment coefficient of the flap generated by pressure. C_{L-p} is the lift force coefficient of the flap generated by pressure. C_{D-p} is the drag coefficient of the flap generated by pressure. T is the time of one pulse period and Δt is the interval time of two adjacent pressure measurements.

The average blowing momentum coefficient C_μ is described as the parameter representing the strength of blowing jet. C_μ can be derived as follows:

$$C_\mu = \frac{1}{T}\sum_{T}\frac{m_j V_j}{\frac{1}{2}\rho_\infty V_\infty^2 S_e}\Delta t \tag{4}$$

where V_j (m/s) is the jet velocity from the blowing slot and m_j is the mass flow rate of the blowing jet, which is measured by a flowmeter set on the upstream of the gas-supply duct. Jet velocity is derived as follows:

$$V_j = \sqrt{\frac{2(P_{0j} - P_j)}{\rho_j}} \tag{5}$$

where P_{0j} and P_j are the total and static pressure, respectively, of the blowing slot and ρ_j is the density of the gas jetting from the blowing slot. Because the Mach number of the jet is lower than 0.3, the jet compressibility is neglected. So ρ_j can be treated as ρ_∞.

The total aerodynamic force/moment of flap can be divided into three components: force/moment provided by pressure, force/moment provided by friction and the reactive force/moment provided by blowing. Friction from the surface of flap is unknown because only the pressure measurement test was taken. Thus, friction influence is ignored in this study. The reactive force of blowing based on momentum equation is as follows:

$$F_b = m_j V_j \tag{6}$$

where F_b is the reactive force of the blowing jet.

Thus, the total aerodynamic force/moment can be derived as follows:

$$C_m = C_{m-p} - C_\mu \tag{7}$$

$$C_L = C_{L-p} + C_\mu \sin\delta_j$$

$$C_D = C_{D-p} - C_\mu \cos\delta_j$$

where C_m is the total pitching moment coefficient of the flap. C_L is the total lift force coefficient of the flap. C_D is the total drag coefficient of the flap and δ_j is the angle between the blowing jet and freestream.

The Strouhal number is the parameter that represents pulsed frequency. The equation of the Strouhal number is as follows:

$$\mathrm{Str} = \frac{fc}{V_\infty} \tag{8}$$

where Str is the Strouhal number. f is the pulsed frequency and c is the chord length of the flap.

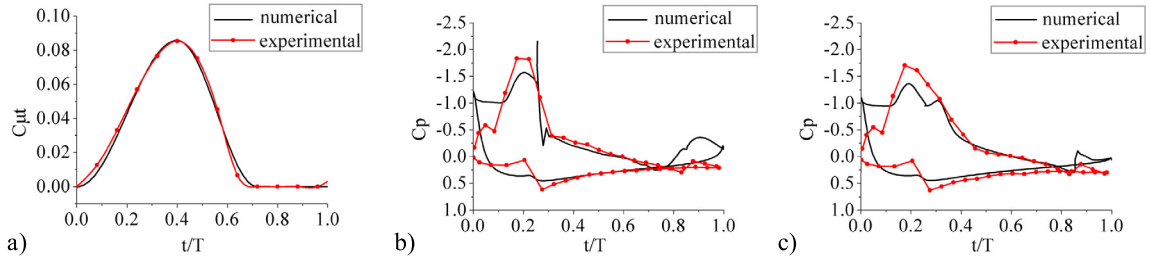

Fig. 10. Comparison between the experimental and numerical results for a) instant blowing momentum coefficient and b) pressure distribution of the flap when $t/T = 0.56$ and c) pressure distribution of the flap when $t/T = 0.8$ ($\alpha = 0°$, $\delta_e = 20°$, $\mathrm{Re} = 0.8 \times 10^6$, $C_\mu = 0.0316$, $\mathrm{Str} = 0.412$).

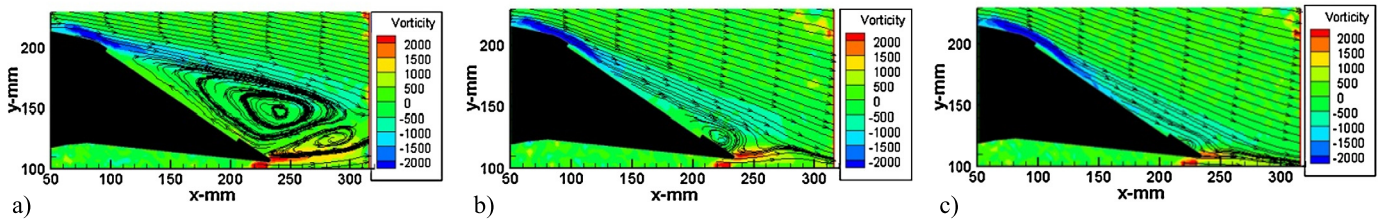

Fig. 11. Continuous blowing effect on the flow structure over the Flap ($\alpha = 0°$, $\delta_e = 20°$, $V_\infty = 20$ m/s, $\mathrm{Re} = 0.8 \times 10^6$) for (a) $C_\mu = 0$, (b) $C_\mu = 0.013$ and (c) $C_\mu = 0.02$.

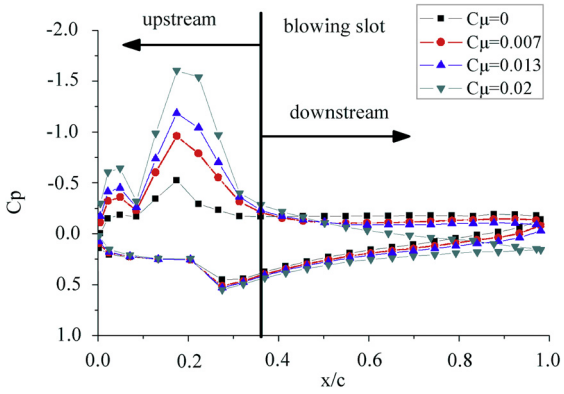

Fig. 12. Continuous blowing effect on the pressure distribution over the flap ($\alpha = 0°$, $\delta_e = 20°$, $V_\infty = 20$ m/s, $\mathrm{Re} = 0.8 \times 10^6$).

2.4. Validation of the numerical simulation results

The numerical simulation method is used in this study to obtain detailed information on flow field. Therefore, the validation of the numerical simulation results is necessary. Fig. 10a shows the evolution of instant blowing momentum coefficient of numerical and experimental results with a 0.0316 blowing momentum coefficient and a 0.412 Strouhal number. Fig. 10b and Fig. 10c show out the pressure distributions on the flap when $t/T = 0.56$ and $t/T = 0.8$, respectively, with a 0.0316 blowing momentum coefficient and 0.412 Strouhal number. The solid line with diamond mark stands for the experimental result, and the solid line without any mark stands for the numerical simulation result. AOA of the main wing is 0° and the deflect angle of the flap is 20° with a 0.8×10^6 Reynolds number. $C_{\mu t}$ and the pressure distributions of $t/T = 0.56$ and $t/T = 0.8$ are well coincided; except for the fore part of the flap, which is covered by the main wing. There is a gap between the main wing and the flap. In experiment, the width of gap is inaccuracy, and in numerical simulation, the width of gap can be set precisely. The width deviation of the gap between the main wing and the flap results in the difference between the numerical and experimental results. Thus, the numerical result can be considered of appropriate and credible.

3. Results and discussion

3.1. Effects of continuous blowing on the flow separation over the flap

Pulsed blowing aims to suppress the flow separation over the flap while less consumption of gas is needed. Therefore, the effect of the continuous blowing on the flow separation can be used as a benchmark to the effect of pulsed blowing.

Fig. 11 and Fig. 12 show the flow field (by PIV) and pressure distribution, respectively, of the flap under different average blowing momentum coefficients when AOA of the main wing is 0°, deflection angle of the flap is 20° and Re is 0.8×10^6. The flow over the flap is completely separated without blowing (see Fig. 11a). When C_μ is 0.013, the separated area is evidently reduced (see Fig. 11b). With the increase of C_μ, the flow over the flap completely reattaches when C_μ is only 0.02 (see Fig. 11c). Fig. 12 shows that a platform area exists on the pressure distribution over the upper surface of flap without blowing (dash line), thereby representing that the flow over the flap is a separated flow. With the increase of C_μ, the platform area of the pressure distribution disappears, and a suction peak occurs near the upstream of the blowing slot. Pressure distribution is divided into two components: the upstream and downstream of the blowing slot. The lift coefficient contribution of these two components is shown in Fig. 13. The lift coefficient of the upstream part is lower than that of the downstream when C_μ is 0. With the increase of C_μ, the lift coefficient of the upstream increases rapidly when the lift coefficient of the downstream decreases slightly. The upstream pressure distribution of the blowing slot contributes 72% of the lift coefficient and, whereas the downstream pressure distribution contributes only 28% when C_μ is 0.02.

3.2. Effect of pulsed blowing on the aerodynamic characteristics of the flap

Fig. 14 shows the pulsed blowing effect on the pitching moment coefficient of the flap changing with the Strouhal number under different averaged blowing momentum coefficient as well as the comparison with that of the continuous blowing under the conditions of $\alpha = 0°$, flap deflection $\delta_e = 20°$, $\mathrm{Re} = 0.8 \times 10^6$. It can be found that:

Under the continuous blowing (with the average blowing momentum coefficient of 0.011, 0.02 and 0.03; $\mathrm{Str} = 0$), the negative

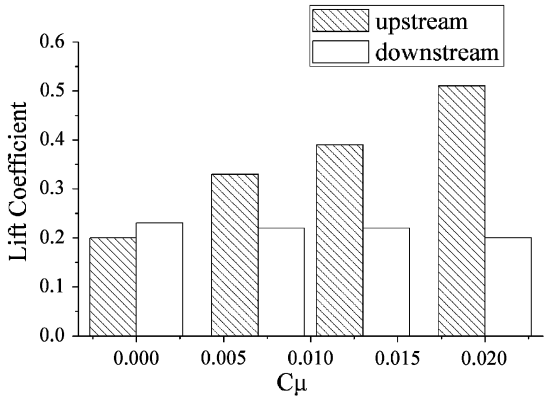

Fig. 13. Proportion of the two components of the lift coefficient of the flap ($\alpha = 0°$, $\delta_e = 20°$, $V_\infty = 20$ m/s, $\mathrm{Re} = 0.8 \times 10^6$).

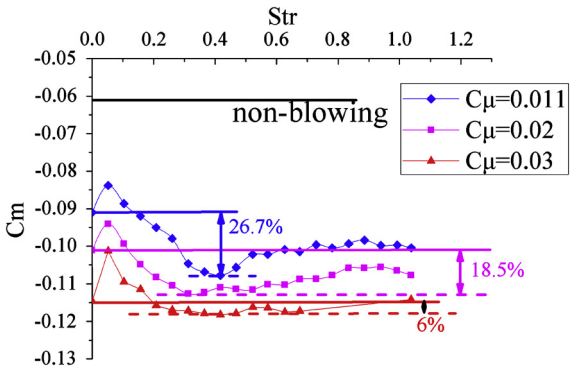

Fig. 14. Pulsed-blowing effect on the pitching moment coefficient of the flap compared with the continuous blowing effect ($\alpha = 0°$, $\delta_e = 20°$, $\mathrm{Re} = 0.8 \times 10^6$).

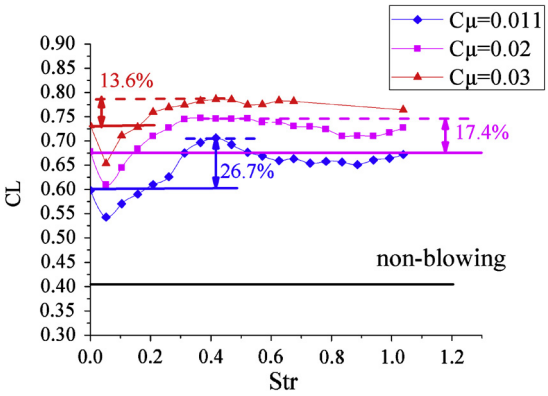

Fig. 15. Pulsed blowing effect on the lift coefficient of the flap compared with the continuous blowing effect ($\alpha = 0°$, $\delta_e = 20°$, $\mathrm{Re} = 0.8 \times 10^6$).

pitching moment coefficient of the flap can be enhanced compared with that of non-blowing. With the continuous blowing momentum coefficient of 0.03, the increment of the negative pitching moment coefficient can be 83% compared with that of non-blowing.

When pulsed blowing acts on the upper surface of flap, the magnitude of pitching moment coefficient is also enhanced. When C_μ is 0.011 (line marked with diamond), the magnitude of pitching moment coefficient decreases slightly with the initial increase of Str and increases rapidly thereafter and reach the maximum value when Str is 0.412 (pulsed frequency of 40 Hz). If Str continuously increases, then the magnitude of pitching moment coefficient decreases slightly. However, the magnitude of the pitching moment coefficient is always greater for the pulsed blowing relative to continuous blowing under the same C_μ if Str is over 0.15 (pulsed frequency of 15 Hz). The maximum increment of the magnitude of pitching moment coefficient with pulsed blowing is 26.7% higher than that of continuous blowing compared with the magnitude of pitching moment coefficient of non-blowing. When C_μ are 0.02 (line marked with square) and 0.03 (line marked with triangle), the maximum increment of the magnitude of pitching moment coefficient with pulsed blowing is 18.5% and 6%, respectively, higher than that of continuous blowing compared with the magnitude of pitching moment coefficient of non-blowing. The difference of the maximum increment of the magnitude of pitching moment coefficient between pulsed and continuous blowing is decreases with the increase of C_μ. When C_μ is sufficiently high, the flow over the flap is completely reattached, and the moment contributed by pressure on the flap surface reaches a threshold value. Thus, the moment contributed by pressure on the flap surface will no longer increase even if C_μ continuously increases after a critical value.

The maximum increment of the magnitude of pitching moment coefficient of the pulsed blowing (compared with that of non-blowing) is 72% when $C_\mu = 0.011$ (see Fig. 14), and the increment of the magnitude of pitching moment coefficient of continuous blowing (compared with that of non-blowing) is 61% when $C_\mu = 0.02$. Thus, by pulsed blowing, gas consumption is nearly only 50% compared with continuous blowing. Accordingly another 11% increment of the magnitude of pitching moment coefficient is acquired. Therefore, pulsed blowing is an advanced control technique that can improve the control efficiency of a control surface, such as a flap, elevator, or aileron.

The preceding analysis indicates that pulsed blowing can increase the pitching moment of the flap, thereby improving its control efficiency. Conversely, pulsed blowing can act as a technique to improve the lift of flap and decrease the drag of flap.

Fig. 15 shows the pulsed blowing effect on the lift coefficient of the flap changing with the Strouhal number under different average blowing momentum coefficient compared with that of continuous blowing. All of the tests have the following conditions: $\alpha = 0°$, flap deflection $\delta_e = 20°$, $V_\infty = 20$ m/s, and $\mathrm{Re} = 0.8 \times 10^6$. It can be found that:

Under continuous blowing (with average blowing momentum coefficient of 0.011, 0.02, and 0.03; Str = 0), the lift coefficient of the flap can be enhanced compared with that of non-blowing. With the continuous blowing momentum coefficient of 0.03, the increment of lift coefficient can be 81% compared with that of non-blowing.

When pulsed blowing acts on the upper surface of flap, the lift coefficient is evidently enhanced. When C_μ is 0.011 (line marked with diamond), the lift coefficient decreases under low Str, and increases rapidly thereafter and reach the maximum value when Str is 0.4 (pulsed frequency of 40 Hz). If Str continuously increases, then the lift coefficient decreases slightly. However, the lift coefficient of pulsed blowing is constantly higher than that of continuous blowing under the same C_μ if Str is over 0.15 (pulsed frequency of 15 Hz). The maximum increment of the lift coefficient with pulsed blowing is 26.7% higher than that of continuous blowing compared with the lift coefficient of non-blowing. When C_μ are 0.02 (line marked with square) and 0.03 (line marked with triangle), the maximum increment of the lift coefficient with pulsed blowing are 17.4% and 13.6%, respectively, higher than that of continuous blowing compared with the lift coefficient of non-blowing. The maximum increment of the lift coefficient between pulsed and continuous blowing decreases with the increase of C_μ. When C_μ is sufficiently high, the flow over the flap is completely reattached, and the lift contributed by pressure on the surface of flap reaches a threshold value. Thus, the lift contributed by pressure on the surface of flap will no longer increase even if C_μ constantly increases after a critical value.

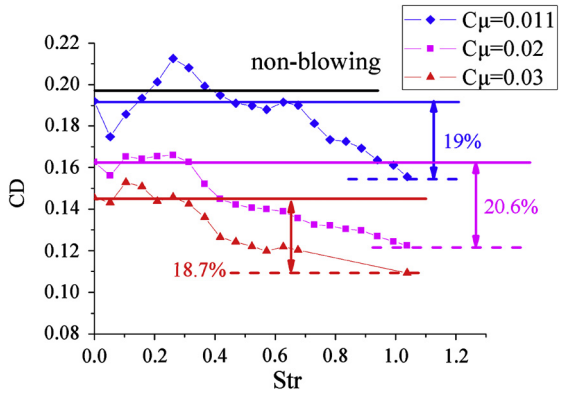

Fig. 16. Pulsed blowing effect on the drag coefficient of flap compared with the continuous blowing effect ($\alpha = 0°$, $\delta_e = 20°$, $\mathrm{Re} = 0.8 \times 10^6$).

Fig. 16 shows the pulsed blowing effect on the drag coefficient of the flap changing with the Strouhal number under different average blowing momentum coefficient compared with that of continuous blowing. All of the tests have the following conditions: $\alpha = 0°$, flap deflection $\delta_e = 20°$, $V_\infty = 20$ m/s, and $\mathrm{Re} = 0.8 \times 10^6$. It can be found that:

Under continuous blowing (with average blowing momentum coefficient of 0.011, 0.02, and 0.03; Str = 0), the drag coefficient of the flap can be reduced compared with that of non-blowing. With the continuous blowing momentum coefficient of 0.03, the decrement of the drag coefficient can be 25% compared with that of non-blowing.

When pulsed blowing acts on the upper surface of flap, the drag coefficient is also evidently enhanced. When C_μ is 0.03 (line marked with triangle), the drag coefficient decreases when Str < 0.05, and increases to the maximum value (even higher than that with continuous blowing) thereafter. If Str continuously increases, the drag coefficient will decrease. However, the maximum decrement of the drag coefficient with pulsed blowing is 18.7% higher than that of continuous blowing compared with the drag coefficient of non-blowing.

3.3. Mechanism of the pulsed blowing control technique

The preceeding discussion emphasized that both continuous and pulsed blowings can improve the aerodynamic performance of the flap. Wu Peng et al. determined that the mechanism of improving aerodynamic performance by continuous blowing is injecting energy into the boundary layer. However, the flow field over the flap is unsteady for the pulsed blowing technique. The mechanism of the pulsed blowing may not be the same as that of continuous blowing.

The numerical simulation results are used in this part. Five sections over flap are selected to study the velocity profile along the flap. A coordinate system of flap is built with the origin set in the leading edge of the flap (see Fig. 17a). Section 1 ($x/c = 0.23$) is set to the upstream near blowing slot ($x/c = 0.24$), and Section 2 ($x/c = 0.26$) is in the downstream near the blowing slot. Section 3 ($x/c = 0.44$), Section 4 ($x/c = 0.72$) and Section 5 ($x/c = 0.97$) are also shown. All of the sections are normal to the surface of the flap.

Fig. 18 shows the evolution of the instant blowing momentum coefficient and instant lift coefficient of the flap during one cycle with $C_\mu = 0.02$ and Str = 0.05 as well as under the following conditions: $\delta_e = 20°$, $V_\infty = 20$ m/s, and $\mathrm{Re} = 0.8 \times 10^6$. $C_{\mu t}$ continuously increases from $t/T = 0$ to $t/T = 0.4$ and the C_{Lt} also increases. From $t/T = 0.4$ to $t/T = 0.65$, $C_{\mu t}$ continuously decreases, but C_{Lt} continuously increases. From $t/T = 0.65$ to $t/T = 0.75$, $C_{\mu t}$ becomes 0, whereas C_{Lt} increase rapidly. After $t/T = 0.75$, C_{Lt} begins to decrease.

Fig. 19 shows the flow structure evolution during one cycle when $C_\mu = 0.02$ and Str = 0.05 under the following conditions: $\delta_e = 20°$, $V_\infty = 20$ m/s, and $\mathrm{Re} = 0.8 \times 10^6$. C_{Lt} represents the instant lift coefficient of the flap. At the beginning of the blowing period ($t/T = 0$), the flow over the flap is completely separated (see Fig. 19a). When $t/T = 0.4$ (see Fig. 19b), the instant blowing momentum coefficient reaches the maximum value. The flow over the flap is reattached, and a suction peak occurs at $x/c = 0.23$. The velocity profile of $x/c = 0.23$ to $x/c = 0.44$ has a high normal gradient, and the velocity magnitude is decreased from $x/c = 0.26$ to $x/c = 0.72$. The flow in $x/c = 0.23$ reattaches because of the

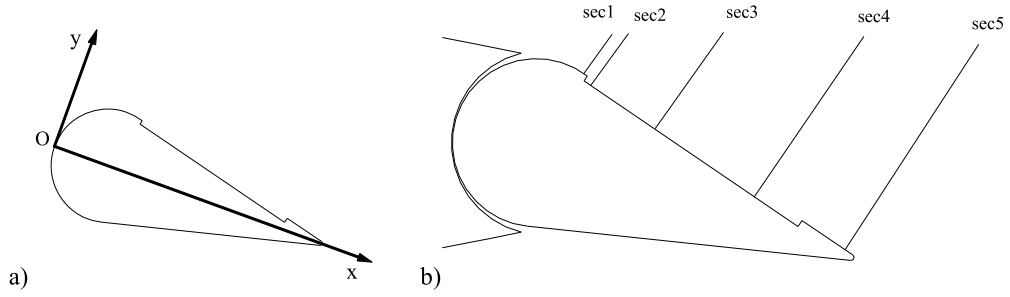

Fig. 17. Velocity profile sections over the flap for a) coordinate system of the flap and b) section location.

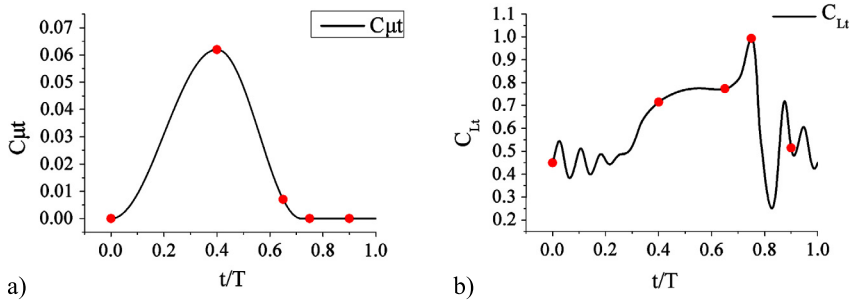

Fig. 18. Evolution of parameter during one cycle for a) instant blowing momentum coefficient and b) instant lift coefficient of the flap ($\delta_e = 20°$, $V_\infty = 20$ m/s, $\mathrm{Re} = 0.8 \times 10^6$, $C_\mu = 0.02$, Str = 0.05).

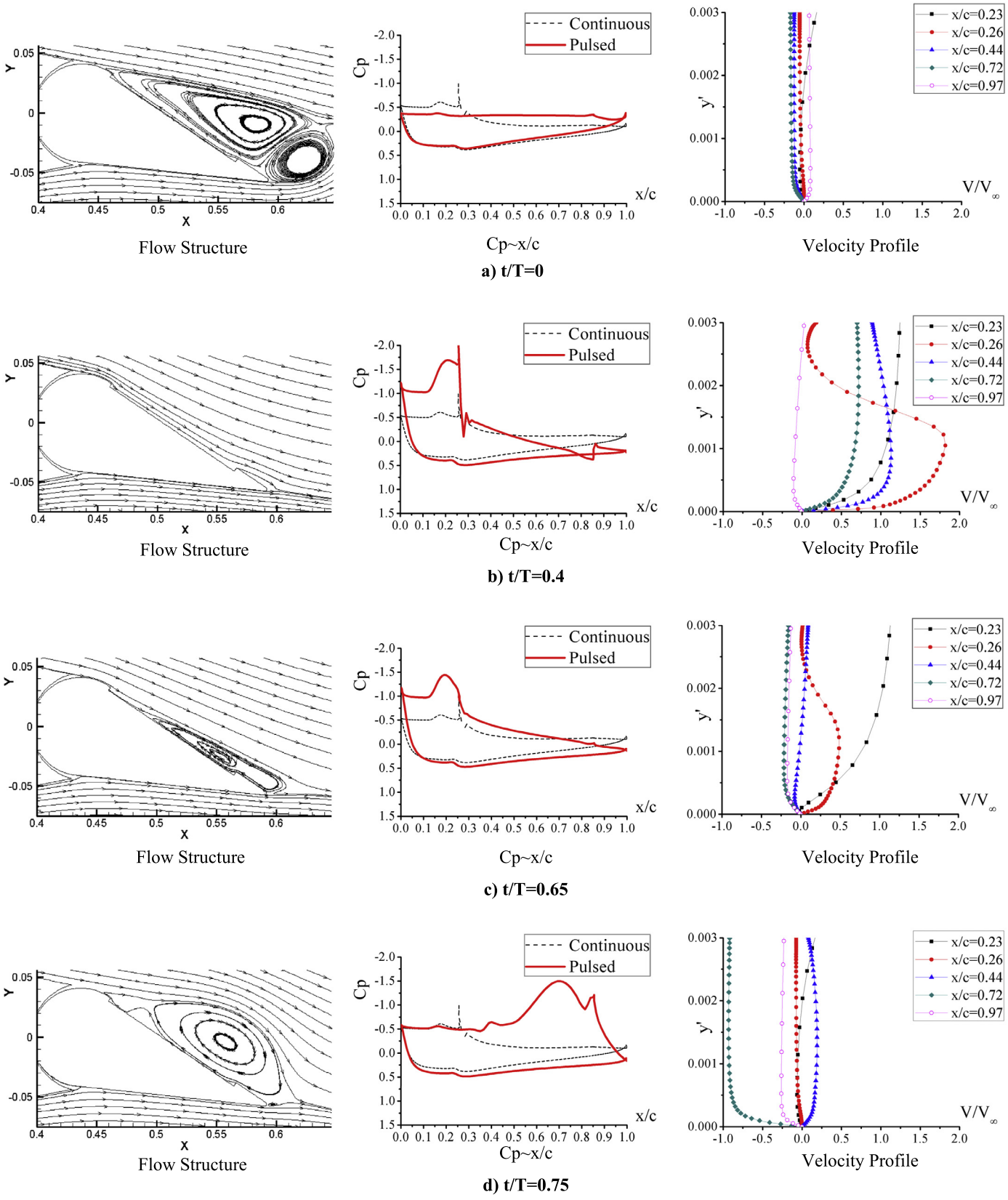

Fig. 19. Flow structure evolution during one cycle with Str = 0.05 ($\delta_e = 20°$, $V_\infty = 20$ m/s, Re = 0.8×10^6, $C_\mu = 0.02$).

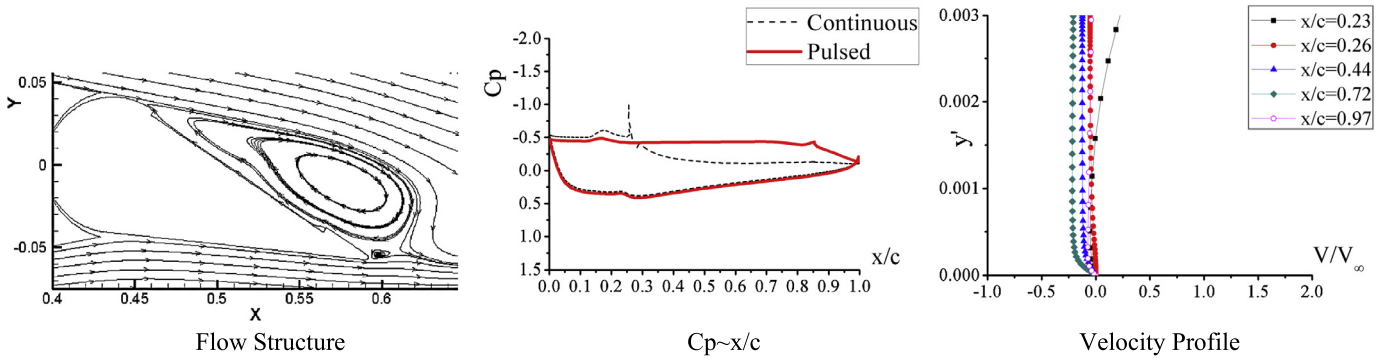

Fig. 19. (*continued*)

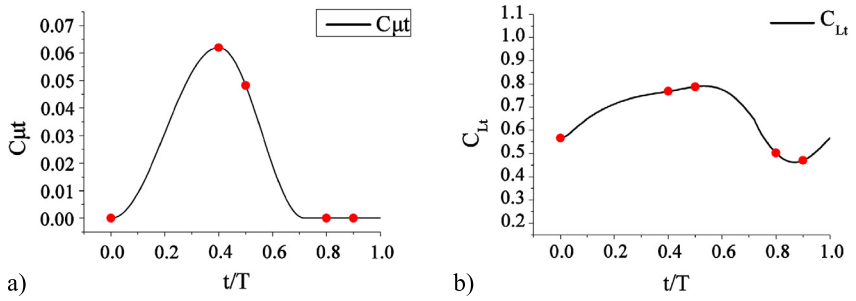

Fig. 20. Evolution of parameter during one cycle for a) instant blowing momentum coefficient and b) instant lift coefficient of the flap ($\delta_e = 20°$, $V_\infty = 20$ m/s, $\mathrm{Re} = 0.8 \times 10^6$, $C_\mu = 0.02$, $\mathrm{Str} = 0.515$).

injection effect, and the flow from $x/c = 0.26$ to $x/c = 0.72$ also reattaches because of the energy offered by the blowing jet. When $t/T = 0.65$ (see Fig. 19c), pulsed blowing goes into the attenuation period and flow over the flap begins to separate from the trailing edge of the flap. However the lift coefficient of the flap constantly increases. A narrow separation area occurs over the flap. The suction peak upstream the blowing slot has attenuated. When $t/T = 0.75$ (see Fig. 19d), a vortex structure covers most of the space over the flap. The suction peak upstream the blowing slot has already disappeared. However the velocity profile of $x/c = 0.44$ has a high normal gradient and high negative velocity magnitude, thereby representing a strong vortex while the velocity magnitude of the other sections is low. When $t/T = 0.9$ (see Fig. 19e), the flow over the flap is completely separated, and the vortex over flap has already broken down. $C_p \sim x$ does not have a suction peak and all velocity profiles of the five sections are nearly maintained at a low normal gradient and magnitude.

According to $C_p \sim x/c$ in Fig. 19, the lift increment of the flap is mainly supplied by the negative pressure of the upstream of the blowing slot in the blowing period. The lift increment of the flap in the non-blowing period is mainly supplied by the vortex induced by the switch from blowing to non-blowing. The velocity profile of $x/c = 0.23$ also shows that a high normal gradient of the velocity profile exists before $t/T = 0.65$.

With the increase of Str, the average lift coefficient of the flap increases. Fig. 20 shows the evolution of the instant blowing momentum coefficient and instant lift coefficient of the flap during one cycle when $C_\mu = 0.02$ and $\mathrm{Str} = 0.515$ under the following conditions: $\delta_e = 20°$, $V_\infty = 20$ m/s, and $\mathrm{Re} = 0.8 \times 10^6$. $C_{\mu t}$ constantly increases from $t/T = 0$ to $t/T = 0.4$ and the C_{Lt} also increases. From $t/T = 0.4$ to $t/T = 0.5$, $C_{\mu t}$ continuously decreases, whereas the C_{Lt} continuously increases. From $t/T = 0.5$ to $t/T = 0.9$, $C_{\mu t}$ constantly decreases and becomes 0, and C_{Lt} begins to decrease.

Fig. 21 shows the flow structure evolution during one cycle when $C_\mu = 0.02$, $\mathrm{Str} = 0.515$ under the following conditions: $\delta_e = 20°$, $V_\infty = 20$ m/s, and $\mathrm{Re} = 0.8 \times 10^6$. At the beginning of the blowing period ($t/T = 0$), a suction peak is present and induced by a vortex near $x/c = 0.35$ (see Fig. 21a). When $t/T = 0.4$ (see Fig. 21b), the instant blowing momentum coefficient reaches the maximum value. The suction peak moves to $x/c = 0.65$. When $t/T = 0.5$ (see Fig. 21c), the suction peak moved to $x/c = 0.72$. The velocity profile of $x/c = 0.72$ has a high normal gradient and a negative velocity magnitude. Thereafter, the moving vortex breaks down after $t/T = 0.8$ (see Fig. 21d and Fig. 21e) and a new suction peak occurs near the blowing slot. Based on $C_p \sim x/c$, a suction peak occurs at the upstream of the blowing slot during an entire period. Simultaneously, a suction peak reduced by a moving vortex occurs on the downstream of blowing slot.

When Str constantly increases, the average lift coefficient of the flap will decrease slightly. Fig. 22 shows the evolution of instant blowing momentum coefficient and instant lift coefficient of the flap during one cycle when $C_\mu = 0.02$, $\mathrm{Str} = 1.65$ under the following conditions: $\delta_e = 20°$, $V_\infty = 20$ m/s, and $\mathrm{Re} = 0.8 \times 10^6$. C_{Lt} variation during the entire period is low.

Fig. 23 shows the flow structure evolution during one cycle when $C_\mu = 0.02$ and $\mathrm{Str} = 1.65$ under the following conditions: $\delta_e = 20°$, $V_\infty = 20$ m/s, and $\mathrm{Re} = 0.8 \times 10^6$. The velocity profile of $x/c = 0.72$ and $x/c = 0.97$ does not change substantially with time, and the velocity magnitude is low. Thus, the flow downstream of $x/c = 0.72$ is separated in the entire period. However, the velocity profile of $x/c = 0.23$ is satiated even if in the non-blowing period. The vortex generated by the switch from blowing to non-blowing does not induce a high suction peak over the flap in the entire period. Most of the lift increment is contributed by the leading edge of the flap.

The preceding discussion emphasized that the mechanism of improving the lift of the flap by pulsed blowing can be described

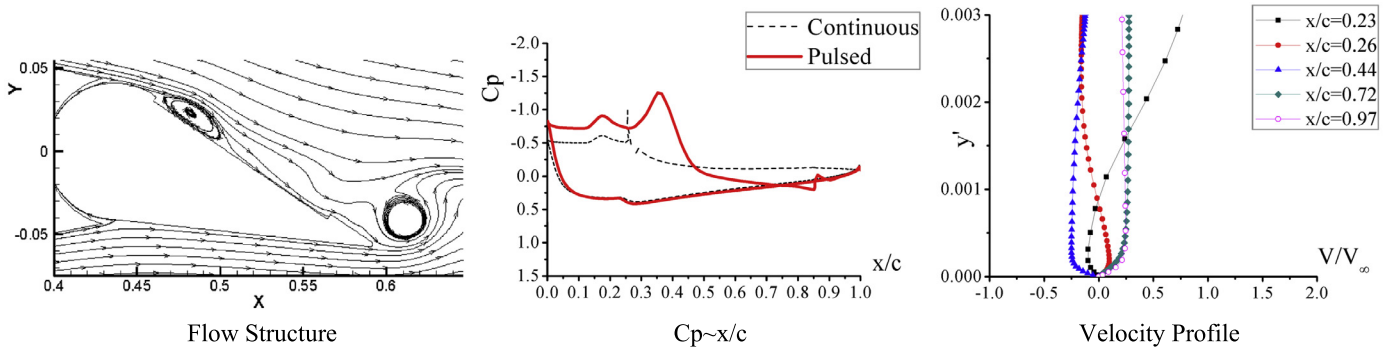

a) t/T=0

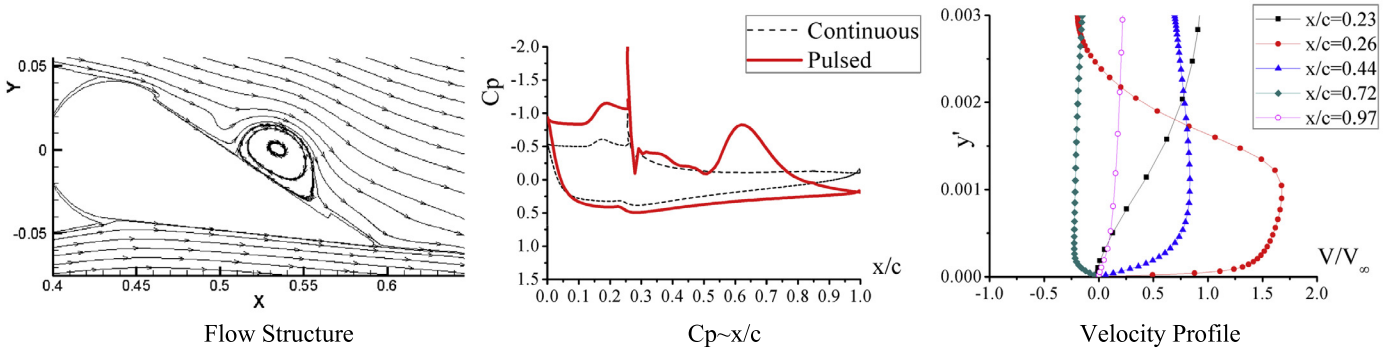

b) t/T=0.4

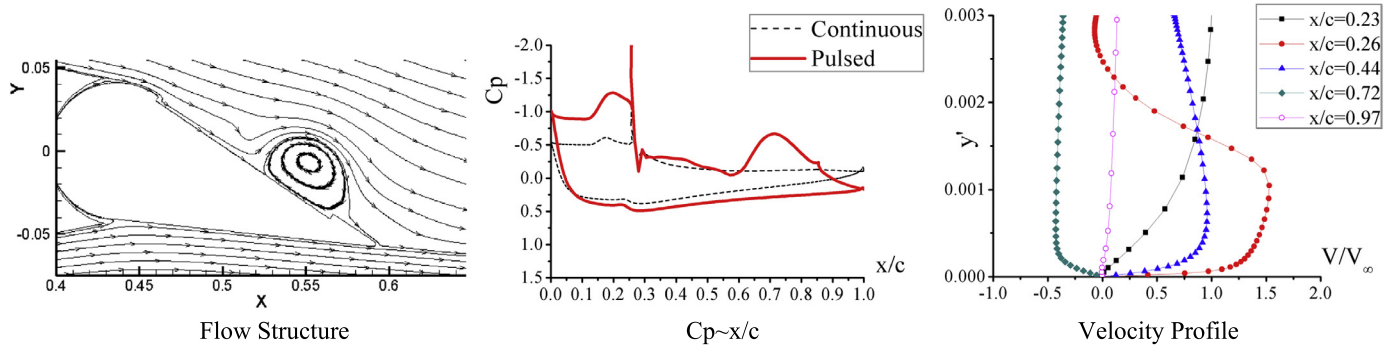

c) t/T=0.5

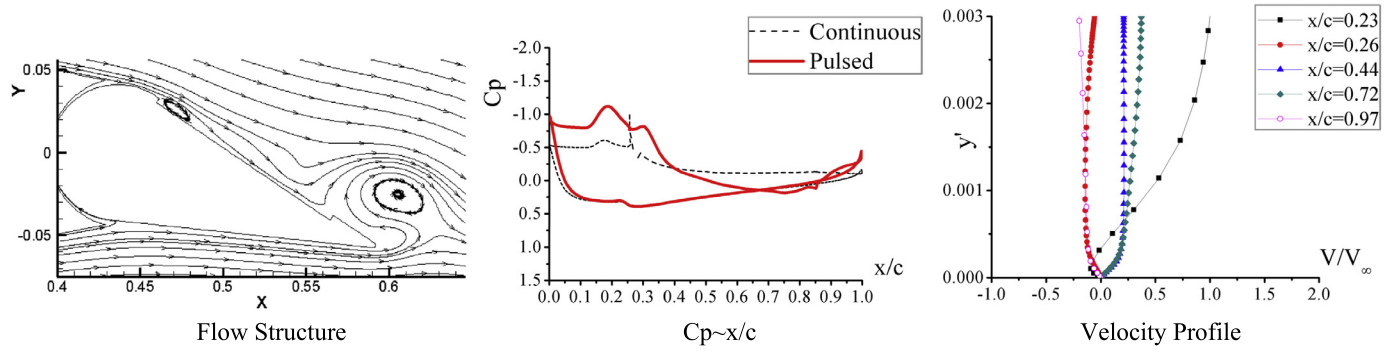

d) t/T=0.8

Fig. 21. Flow structure evolution during one cycle with Str = 0.515 ($\delta_e = 20°$, $V_\infty = 20$ m/s, Re = 0.8×10^6, $C_\mu = 0.02$).

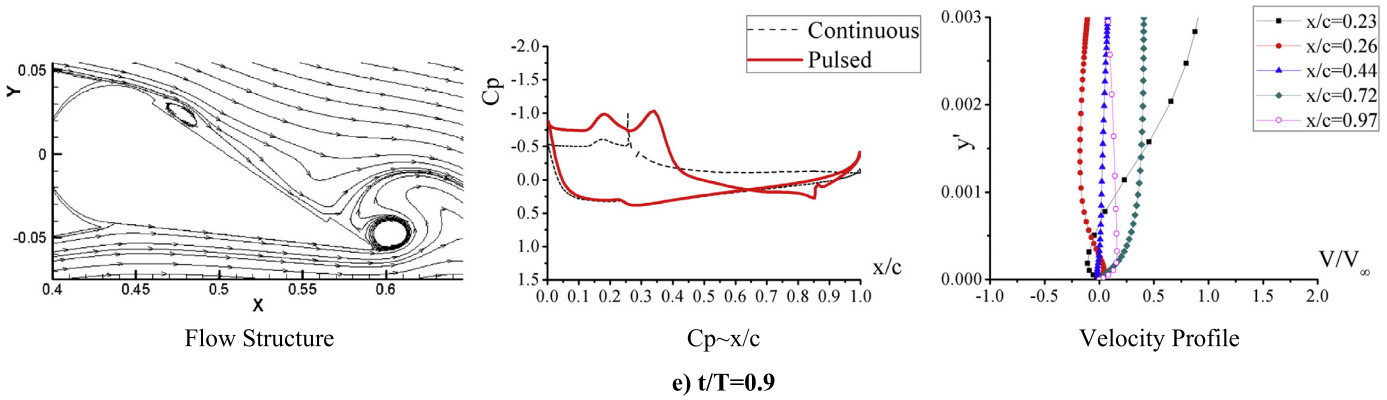

e) t/T=0.9

Fig. 21. (*continued*)

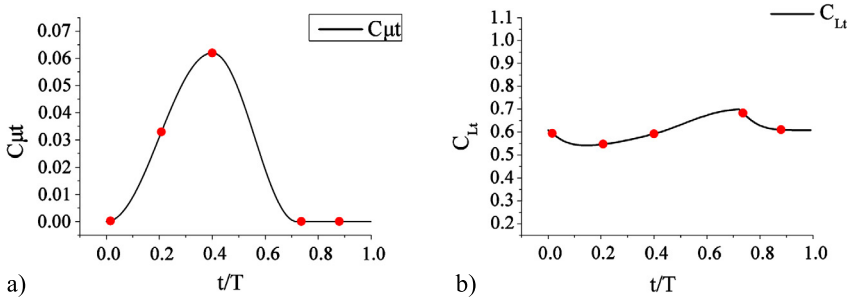

Fig. 22. Evolution of parameter during one cycle for a) instant blowing momentum coefficient and b) instant lift coefficient of the flap ($\delta_e = 20°$, $V_\infty = 20$ m/s, $\mathrm{Re} = 0.8 \times 10^6$, $C_\mu = 0.02$, $\mathrm{Str} = 1.65$).

as follows: blowing jet can be treated as an injector. The flow upstream of the blowing slot is injected by the blowing jet and induces a suction peak of pressure, which is the same mechanism as continuous blowing. Conversely, the vortex generated by the switch of blowing and non-blowing over the blowing slot induces a suction peak of pressure. Lift increment is generated by these two components of suction peak. Both the inject effect and the vortex need sufficient time to develop. When Str is low, the lift increment supplied by the inject effect can reach its maximum value and stability. The lift increment supplied by the vortex reaches the maximum value and decreases thereafter. Thus, Str has a critical value that balances the both components of lift increment and leads their sum into maximum value. When Str is higher than the critical value, the vortex generated by the switch from blowing and non-blowing cannot obtain sufficient time to develop, thereby leading to a lift increment penalty. Moreover, the blowing jet cannot induce a high speed-up in the upstream of the blowing slot, thereby leading to a lift increment penalty.

4. Conclusions

Several conclusions are drawn based on the preceding analyses.

This study introduces an innovative flow control technique, namely, pulse blowing technique. Evidently, flow separation can be suppressed by pulsed blowing and the control efficiency of the flap can be enhanced.

With the increasing Str of pulsed blowing, the increment of lift and the magnitude of pitching moment increases gradually and a critical Str exist in which the increment of the lift and the magnitude of pitching moment coefficient reaches the maximum value. The critical Str is decided by the velocity of freestream and the geometry of model.

The pulsed blowing effect is larger than that of continuous blowing when Str is larger than the critical Str. In the experimental test, the largest increment of the magnitude of pitching moment coefficient is obtained when Str is approximately 0.4 ($f = 40$ Hz). This result shows that the increment of the magnitude of pitching moment coefficient with pulsed blowing is 26.7% larger than that of continuous blowing under the same blowing momentum, that is, $C_\mu = 0.011$ and $V_\infty = 20$ m/s. The maximum increment of the magnitude of pitching moment coefficient of pulsed blowing with $C_\mu = 0.011$ is 72%, and the increment of the magnitude of pitching moment coefficient of continuous blowing with $C_\mu = 0.02$ is 61%. Thus, by pulsed blowing, gas consumption is only 50% compared with continuous blowing, and another 11% increment of the magnitude of pitching moment coefficient is acquired. Therefore, pulsed blowing is an advanced control technique that can be used to improve the control efficiency of the flap.

The mechanism of improving the lift of the flap by pulsed blowing can be divided into two components. First, blowing jet can be treated as an injector. The flow upstream of the blowing slot is injected by the blowing jet and induces a suction peak, which is the same mechanism as continuous blowing. Second, the vortex generated by the switch of blowing and non-blowing over the blowing slot induces a suction peak. Lift increment is generated by these two components of suction peak. Both the inject effect and vortex need sufficient time to develop. When Str is low, the lift increment supplied by the inject effect can reach its maximum value and stability. The lift increment supplied by the vortex reaches the maximum value and decreases thereafter. A critical value of Str balances the both components of the lift increment and leads their sum into maximum value. When Str is higher than the critical value, the vortex generated by the switch from blowing and non-blowing cannot obtain sufficient time to develop, thereby leading to a lift increment penalty in the non-blowing period. By contrast, the blowing jet cannot induce a high speed-up in the upstream of blowing slot, thereby leading to a lift increment penalty in the blowing period. Therefore, the most important parameters of the pulsed blowing control technique are C_μ and Str. C_μ masters the

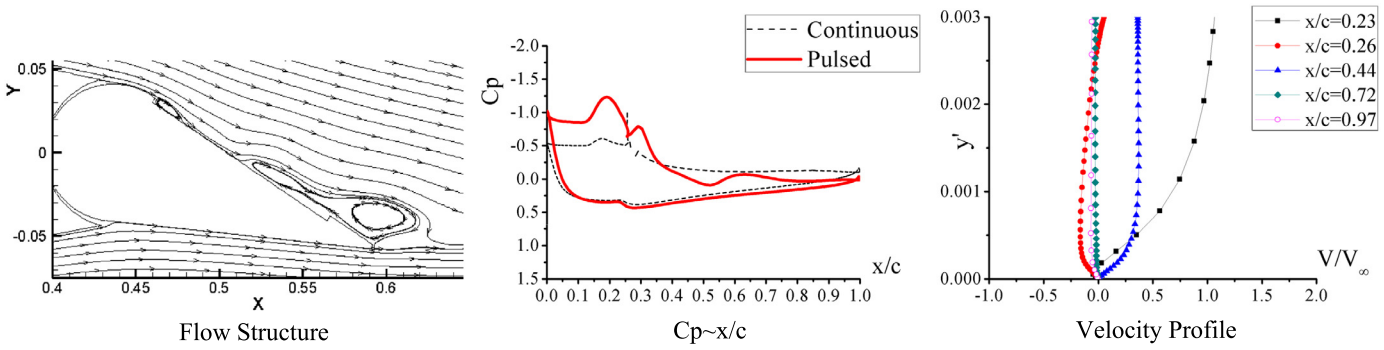

a) t/T=0.016

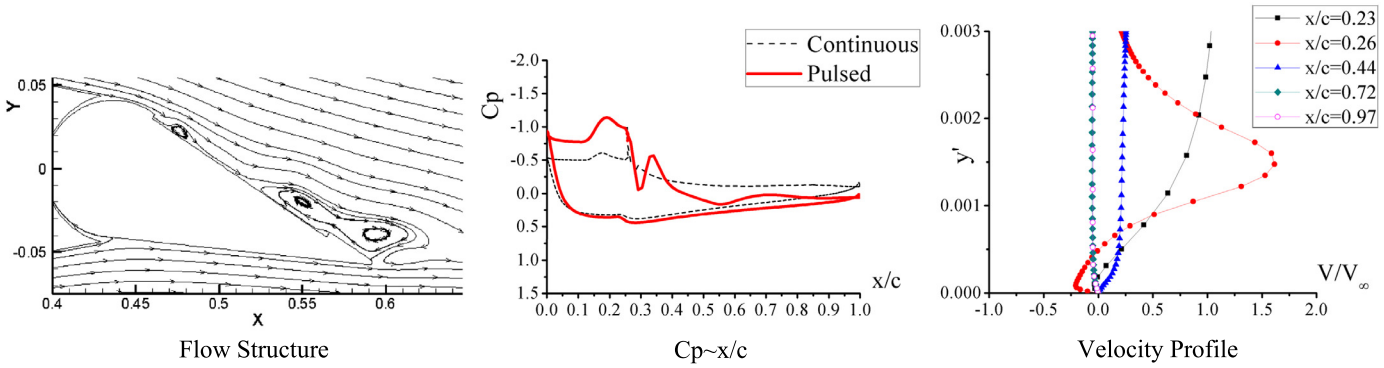

b) t/T=0.208

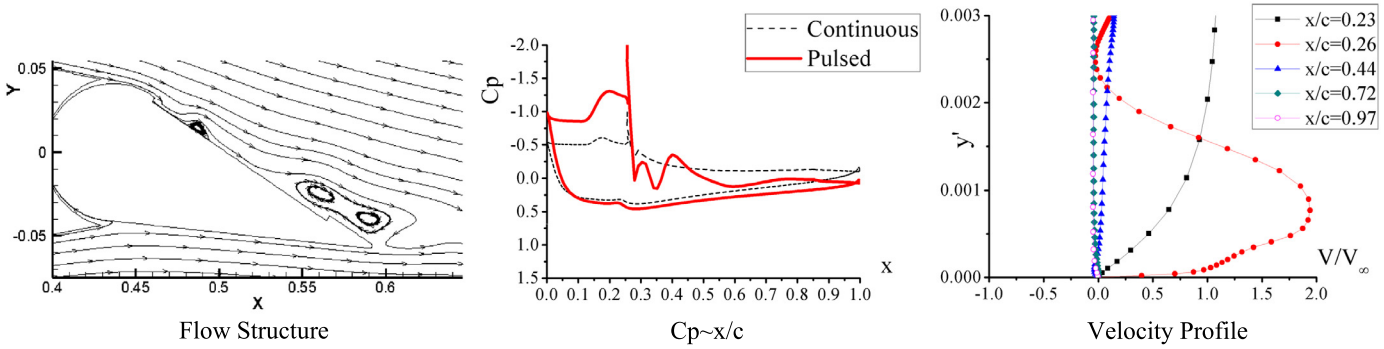

c) t/T=0.4

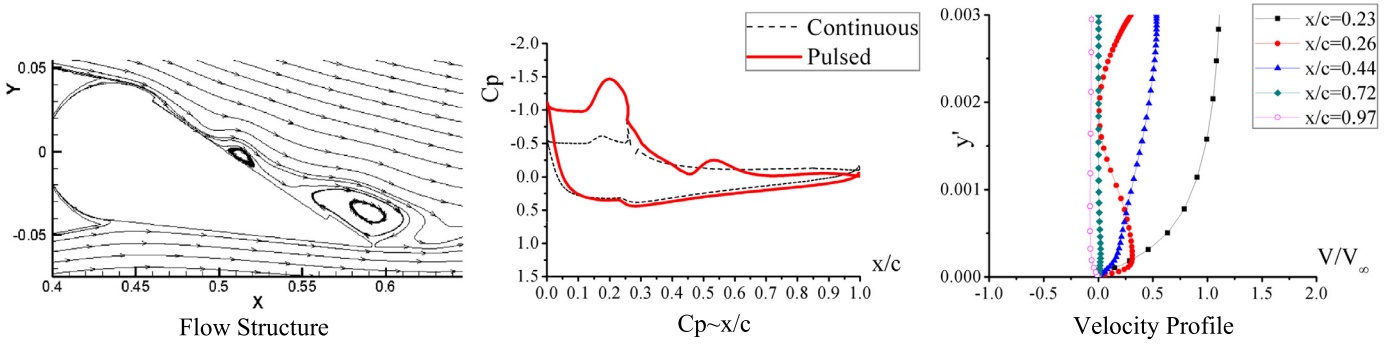

d) t/T=0.736

Fig. 23. Flow structure evolution during one cycle with Str = 1.65 ($\delta_e = 20°$, $V_\infty = 20$ m/s, Re = 0.8×10^6, $C_\mu = 0.02$).

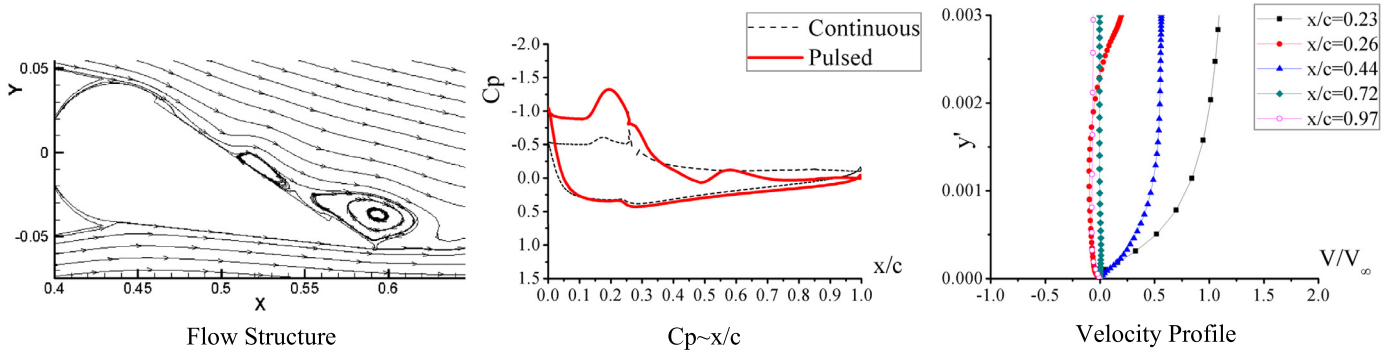

e) t/T=0.88

Fig. 23. (*continued*)

suction peak upstream the blowing slot and Str masters the suction peak downstream the blowing slot.

Conflict of interest statement

There is no conflict of interest.

Acknowledgements

The research work was supported by the National Natural Science Foundation of China (11272035), the Aeronautical Science Foundation of China (2011ZA51003).

References

[1] W.L. Sellers III, B.A. Singer, L.D. Leavitt, Aerodynamics for revolutionary air vehicles, in: 21st AIAA Applied Aerodynamics Conference, June 2003, AIAA Paper 2003-3785.
[2] V.J. Modi, S.R. Munshi, G. Bandyopadhyay, T. Yokomizo, High-performance airfoil with moving surface boundary-layer control, J. Aircr. 35 (4) (1998) 544–553.
[3] A. Asrokin, M.R. Ramly, A.H. Ahmad, Rotating cylinder design as a lifting generator, in: 2nd International Conference on Mechanical Engineering Research, July 2013.
[4] Y.Y. Zhang, D.G. Huang, X.J. Sun, G.Q. Wu, Exploration in optimal design of an airfoil with a leading edge rotating cylinder, Int. J. Therm. Sci. 19 (4) (2010) 318–325.
[5] A. Salmasi, A. Shadaram, A.S. Taleghani, Effect of plasma actuator placement on the airfoil efficiency at poststall angles of attack, IEEE Trans. Plasma Sci. 41 (10) (2013) 3079–3085.
[6] J.J. Wang, K.S. Choi, L.H. Feng, T.N. Jukes, R.D. Whalley, Recent developments in DBD plasma flow control, Prog. Aerosp. Sci. 62 (1) (2013) 52–78.
[7] T.C. Corke, C.L. Enloe, S.P. Wilkinson, Dielectric barrier discharge plasma actuators for flow control, Annu. Rev. Fluid Mech. 42 (1) (2010) 505–529.
[8] N.M. Houser, L. Gimeno, R.E. Hanson, T. Goldhawk, T. Simpson, P. Lavoie, Microfabrication of dielectric barrier discharge plasma actuators for flow control, Sens. Actuators A, Phys. 201 (1) (2013) 101–104.
[9] G.C. Zha, W. Gao, C.D. Paxton, Jet effects on coflow jet airfoil performance, AIAA J. 45 (6) (2007) 1222–1231.
[10] H.S. Im, G.C. Zha, B.P.E. Dano, Large eddy simulation of coflow jet airfoil at high angle of attack, J. Fluids Eng., Trans. ASME 136 (2) (2014) 1101–1111.
[11] B.Y. Wang, G.C. Zha, Detached-eddy simulation of a coflow jet airfoil at high angle of attack, J. Aircr. 48 (5) (2011) 1495–1502.
[12] W.B. Gan, Z. Zhou, X.P. Xu, R. Wang, Delayed detached-eddy simulation and application of a coflow jet airfoil at high angle of attack, Adv. Comput. Model. Simul. 444 (1) (2014) 270–277.
[13] Peng Wu, Xue Ying Deng, Yan Kui Wang, Application of pulsed blowing technique in high-lift control surface design, Adv. Mater. Res. 482 (1) (2012) 121–125.
[14] A. Seifert, A. Darabi, I. Wygnanski, Delay of airfoil stall by periodic excitation, J. Aircr. 33 (4) (1996) 691–698.
[15] David Greenblatt, Israel J. Wygnanski, The control of flow separation by periodic excitation, Prog. Aerosp. Sci. 36 (2000) 487–545.